Experimental and Numerical Investigations on Aero-Thermal Interaction of Cooling Air Ejected from Multiple Cooling Holes

2013 MARCH

Post Graduate School Of Engineering

Iwate University

Mohammad Kamil bin Abdullah

Table of Contents

List of Figures

List of Tables

Abstract

"Film cooling is the introduction of secondary fluid (coolant) at one or more discrete locations along a surface exposed to a high temperature environment to protect that surface not only in the immediate region of injection but also in the downstream region," (Goldstien, 1971). The secondary air which is cool air were extracted from the compressor and injected near the blade surface (through holes or slots) to provide a layer of cool fluid between the hot gases and the blade surface thus reducing the heat transfer to the surface. Enormous numbers of experimental and computational investigations dealing with both the aerodynamic and the thermal aspect of film cooling have been made available ever since. At the early stage of its introduction, the experimental investigations were usually focused on either thermal or aerodynamic aspect of the study. However, with the introduction of the laser based measurement (PIV and LDV), which reduce the complexity of aerodynamic measurements, most of current literature involving film cooling will have both, the thermal and the aerodynamic aspect of the study. Most of the available literature involved a discrete hole or single row cooling hole with common hole inclination angle towards the streamwise direction at 30° and 35°. Although earlier researches have proved that decreasing the hole inclination angle could provide better film cooling performance, there are very few literature available with regards the hole inclination angle lower than 30°. Based on these facts, the present study intended to investigate the aero-thermal interaction of a multiple shallow hole angle. In addition to the experiments, computational investigation has been extensively used in particular to explore the potential of new hole geometries and configurations. The computational investigation has also been manipulates to provide the physical insight of the aero-thermal interaction of the study.

The present study involves thermal and aerodynamic investigations of multiple cooling holes with shallow hole angle. Total of three test models are considered in the present study namely TMA, TMB and TMG. The base line test model; TMB is design to justify the commonly used cooling hole having 35° hole angle. The other two test models; TMA and TMG, are having a shallow hole angle of 20° with different lateral pitch distance of 6D and 3D, respectively. Total of twenty conventional cylindrical holes constituting a matrix composed of four rows with five holes in each row. Thermal and aerodynamic investigations are carried out involving all of the test models. The thermal investigations involve

temperature measurement of test model surface by infrared thermography; NEC/Avio H2640. The surface temperature is converted to film cooling effectiveness to represent the thermal performance of the given test model. In addition to the surface temperature measurements, the thermal investigations also involve measurement of thermal field downstream of each row cooling hole. The thermal fields are measured by a thermocouple rig which is mounted on a 2-D traverse system. The traverse system will navigate the rig according to a designated measurement grid to enable thermal field contour plot. 3-D Laser Doppler Velocimetry has been utilized for the aerodynamic measurements. The laser probes are mounted on a 3-D traverse system which will navigate the probes according to a designated measurement grid to enable velocity field contour plot. The measurements are carried out at single Reynolds number base on the hole diameter of 6200 at three different blowing ratios of 0.5, 1.0 and 2.0. The present study also includes the numerical investigation of the above mentioned cases. Simplified computational domains are constructed to include only single lateral pitch based on the test models. The meshes are generated by ANSYS ICEMCFD ver. 12. The analyses are carried out by ANSYS CFX ver.12 with the employment of steady and unsteady Reynolds Average Navier Stokes analyses using the shear stress transports turbulence model.

The experimental aerodynamic results are presented in the form of contour plot of various variables including film cooling effectiveness, normalized u, v, and w velocities. The velocity distributions show that at BR = 1.0, the lift-off effects are more apparent in the case of TMB in comparison with the TMA. The vector plots between the two test models also reveals the different in terms of the positioning of the counter rotating vortex core which is observed to be further away from the wall surface in TMB. The velocity plots also reveal that downstream of the cooling hole at the centerline, TMA is having higher streamwise velocity in comparison with TMB. These observations can be directly associated with the different in the inclination angle of the cooling hole. Steeper angle in the case of TMA allowed more streamwise momentum component to be ejected through the cooling hole in comparison with the case of TMB. The computational fluid dynamics investigation also reveals the occurrence of different flow structure inside the cooling hole between TMA and TMB. In the case of TMB, the separation which occurs at the inlet of the cooling hole triggers the formation of counter rotating vortex inside of the cooling hole and persists through the cooling hole. An accomplish counter rotating vortices can be observed at various plane inside the cooling hole. The same observation cannot be made for TMA, where the vector plot reveals that the

secondary air which has been separated at the cooling hole inlet then reattached to the downstream wall of the cooling hole. This phenomenon hinders the formation of counter rotating vortex inside of the cooling hole which will only be completed by the cross-flow phenomena after the secondary air exiting the cooling hole. In comparison between TMA and TMG, both the experimental and computational results reveal that the shorter lateral pitch in TMG allows the secondary air to dominate the lateral space between cooling hole. The domination of the secondary air within the lateral space leads to greater blockage not only at the hole vicinity but also at the lateral space. The numerical results also show that the greater blockage which occur in TMG resulting a different interaction between the upcoming and the concurrent vortex cores in comparison with TMA. At wider lateral pitch of TMA, the upcoming vortex cores diffuse directly into the concurrent vortex cores keeping the secondary air in-line. At shorter lateral pitch of TMG, the upcoming vortex cores are deflected in the lateral direction before diffuse at further downstream of the cooling hole. The deflection cause the secondary air to disperses at the lateral space. The velocity plots also confirmed the interaction between the neighboring counter rotating vortices in the case of TMG which hindering it own growth and leads to lesser lift-off effects.

The thermal investigations results are presented in terms of the contour plot of film cooling effectiveness, distribution of laterally average film cooling effectiveness and area average film cooling effectiveness along the x-axis. Benchmarking between the present and previous study are made to validate the present measurement and analysis approach. Good agreement has been achieved between the present and previous study. The film cooling effectiveness provided by TMA is higher at all blowing ratio in comparison with TMB particularly at BR=1.0 and 2.0. The thermal fields show that at BR=1.0, the lift-off effects are more evident in the case of TMB in comparison with TMA. At BR=2.0, the thermal fields show complete detachment of the secondary air from the wall for the case of TMB leaving no trace of film cooling coverage on the surface. The thermal fields also indicate a lesser dispersion of the thermal field in the case of TMA in comparison with TMB which can directly be associated with the interaction rate between the secondary air and the mainstream air. In comparison between TMA and TMG, similar distribution of film cooling coverage can be observed downstream the first and second row cooling hole. Downstream the third and fourth row cooling hole, TMG start to provide better film cooling coverage. The contour plot shows an establishment of full coverage film cooling effectiveness region accommodating the

lateral space between the cooling hole centerline. This observation serves the flow phenomena which have been describe earlier in the writing. The thermal fields also show the domination of the secondary air in the lateral space which is more apparent downstream of the third and fourth row cooling hole.

Conclusions of the present study are summarized as follows; a) shallow hole angle configurations are definitely improving the film cooling coverage in comparison to the commonly used hole angle at 30° or 35°. The superiority of the shallow hole angle is more apparent at higher blowing ratio cases in which the cooling protection provided at BR = 2.0 of shallow hole angle is a match to the result of BR = 2.0 of the 35° hole angle; b) at shorter lateral pitch distance, full coverage film cooling effectiveness were prevail indicating the benefit of the interaction between the secondary air of the neighboring cooling holes; c) the superposition effect induces by the in-line hole arrangement of the present study help to improve the film cooling performance with greater benefit were obtained by the shallow hole angle in comparison to the 35 degree hole angle; d) the CFD results confirm the formation of a counter rotating vortex pair inside of the cooling hole which perseveres until downstream of the cooling hole in all cases. Increase in the length of the cooling hole will allow the separated secondary air to reattach thus hindering the formation of the kidney vortices so as to better the film cooling effectiveness in the case of TMA and TMG; e) the domination of the mainstream air at the lateral space between the cooling hole in the case at longer lateral pitch distance kept the secondary jet in-line as it travel towards the downstream direction. It will cause the upcoming vortex core to directly infuses thus amplify the jetting effect of the downstream vortices which will ultimately minimizing the utilization of the secondary air; f) at the shorter lateral pitch distance, the narrow lateral space between the cooling hole enables the secondary air jet to interact with each other and prevent the mainstream air to dominating the lateral space resulting the upcoming vortices to be deflected while it approaching the downstream cooling hole. At the same time, the deflection helps to spread the secondary air laterally hence to better the film cooling effectiveness.

Chapter 1

Introduction

This chapter provides the background history on the gas turbine and the present progress of the technology. The background section intends to establish the important of gas turbine cooling technologies in the present gas turbine performance. The chapter also consists of a literature review section which is focusing on the literature related to flat plate film cooling technology investigation covering the empirical and numerical aspects. In addition, this chapter also addresses the research motivation, research objectives and research framework involve in the present study.

1.1 Background

The history shows that the interest and development of gas turbine can be traced back to over a century and half ago. However, the history of the gas turbine as a viable energy conversion device had only began with Frank Whittle's patent award on the jet engine in 1930 and his static test of a jet engine in 1937. Shortly thereafter, in 1939, Hans von Ohain led a German demonstration of jet-engine-powered flight, and the Brown Boveri company introduced a 4-MW industrial gas turbine producing electrical power in Neuchatel, Switzerland. Since then, gas turbine has been a success stories employed by the aircraft and the stationary power plant till today. Figure 1 illustrates the industrial gas turbine structure of 7F 5-Series gas turbine manufactured by General Electric. In general, the gas turbine consists of three main components; compressor, combustor and turbine. The incoming air is

compresses by multistage stage compressor producing high pressure air to be supplied to the combustor. The high pressure air is mixes with the fuel and burns inside the combustor and produces high pressure, high temperature and high velocity gas. The turbine at the later stage will extracts the energy from the gas before being converted to necessary energy required.

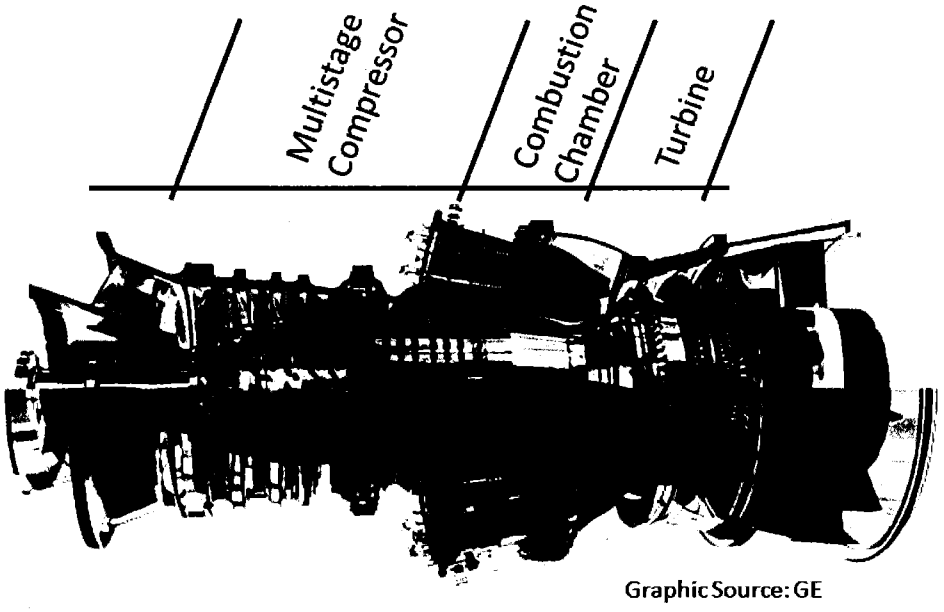

Figure 1 Industrial Gas Turbine

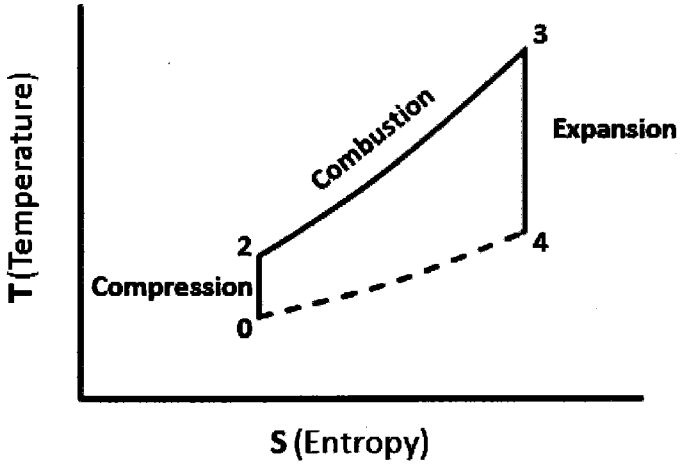

Figure 2 Temperature–Entropy Plot of Ideal Brayton Cycle

Gas turbine operation is based on fundamental thermodynamic cycle known as Brayton Cycle. Figure 2 shows the temperature–entropy diagram for the ideal Brayton cycle representing a closed cycle gas turbine. The cycle consists of an isentropic compression of the gas from state 0 to state 2; a constant pressure heat addition to state 3; an isentropic expansion to state 4, in which work is done; and an isobaric closure of the cycle back to the initial state. The overall efficiency of the Brayton Cycle can be define as Eq. 1,

$$\eta = \frac{W_{net\ 3\to4}}{Q_{in\ 3\to2}} = 1 - \left(\frac{T_4}{T_3}\right) \tag{1}$$

where;

$W_{net\ 3\to4}$, the net work produce by the cycle [W]

$Q_{in\ 3\to4}$, the heat supplied to the cycle [W]

T_3 , inlet temperature of the turbine [K], and;

T_4 , exit temperature of the turbine [K]

Referring to Eq. 1, higher turbine inlet temperature, T_3 will yield higher overall thermal efficiency of the cycle. Increasing turbine inlet temperature has been the main approach to improve the overall performance of a gas turbine.

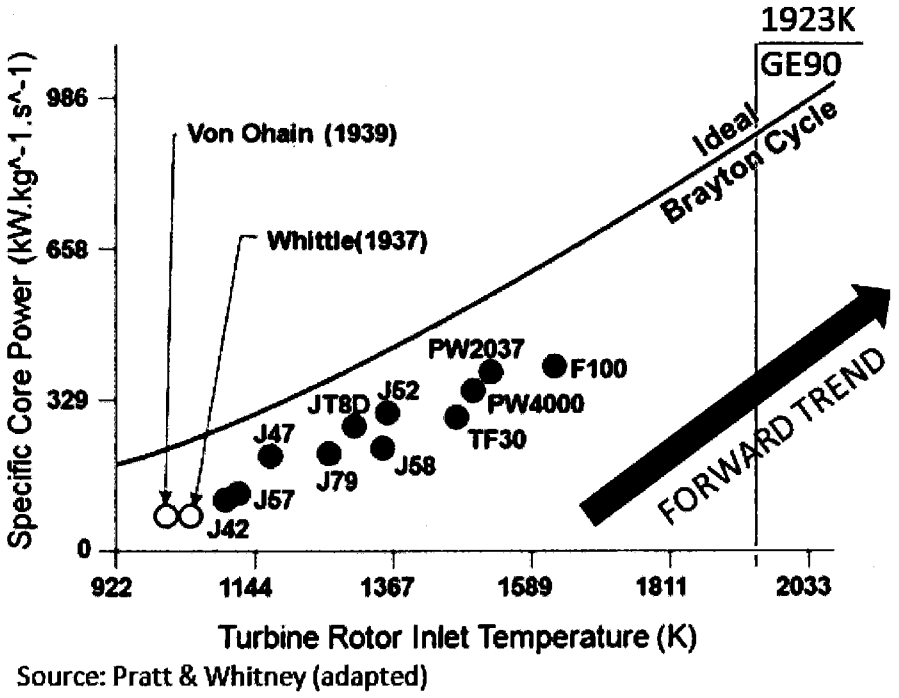

Figure 3 Historical Progress on Turbine Inlet Temperature

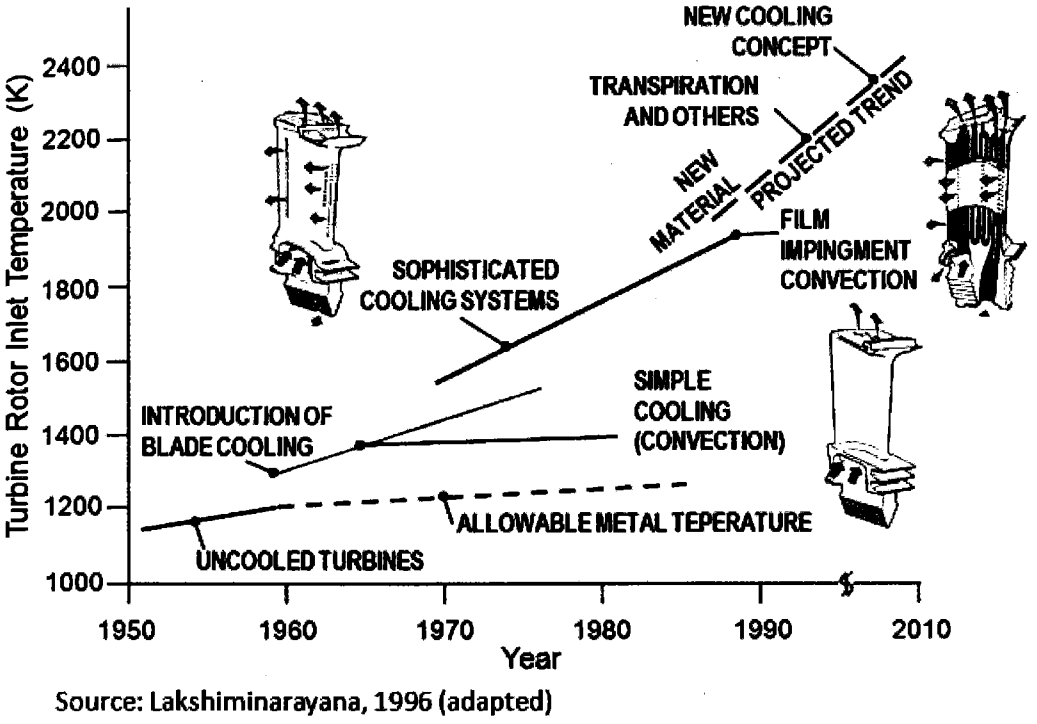

Figure 4 Blade Cooling Revolution

As the demand for better performance gas turbine increases, the turbine inlet temperature has been push far exceeding the operating temperature condition of the turbine components material. Most of the present generation gas turbines are operated at turbine inlet temperature in the range of 1800K to 2000K which is much higher than the melting temperature of the available alloys used to make the turbine components; blade, vanes, combustor wall, etc. Figure 3 shows the progress of the turbine inlet temperature from the time of Whittle and Von Ohain to the present. The figure also marks the present turbine inlet temperature of GE90 at 1923K. The increase of the turbine inlet temperature has been made possible by the employment of cooling scheme on the turbine components as shown in Figure 4. There are many different cooling techniques that have been devised and implemented to provide necessary protection of the turbine components. Turbine blade as one of the critical turbine components for example consist of complicated cooling scheme including thermal barrier coating, internal convective cooling, impingement cooling, and external cooling also known as film cooling. Extensive review of the overall heat transfer and cooling technology can be found in Han et al. [1].

At the early stage, turbine blade has been cooled mainly by the internal convection in which the coolant is passes through the blade from the hub and releases at the blade tip. To maximize the utilization of the coolant, film cooling has been introduced in which, the coolant will be injected from the blade surface through a cooling hole. The injected coolant will performs a thin film layer of cool fluid avoiding direct contact between the blade surface and the hot gases. Since its introduction, film cooling has been recognized as one of the effective cooling method for the turbine blade and has been used extensively in the present turbine blade design. Figure 5 shows the film cooling hole distribution in the real turbine blade structure. The film cooling has not only been employed on the blade surface but also on the end wall of the turbine blade to provide necessary cooling protection for the component.

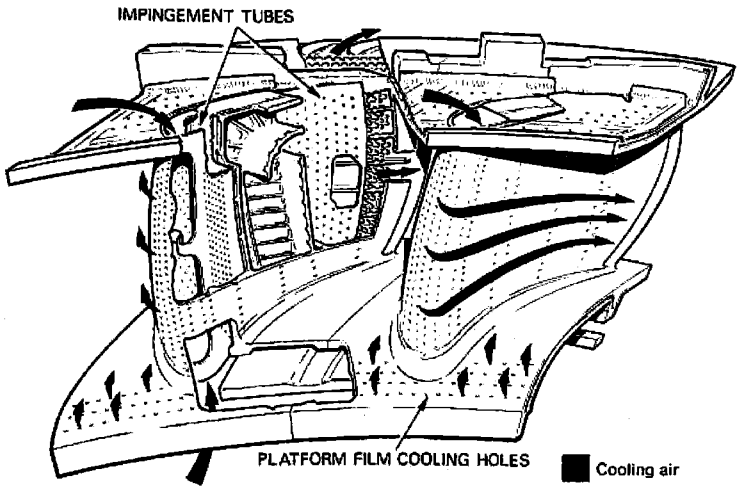

Figure 5 Film Cooling Holes Employed by the Turbine Blade

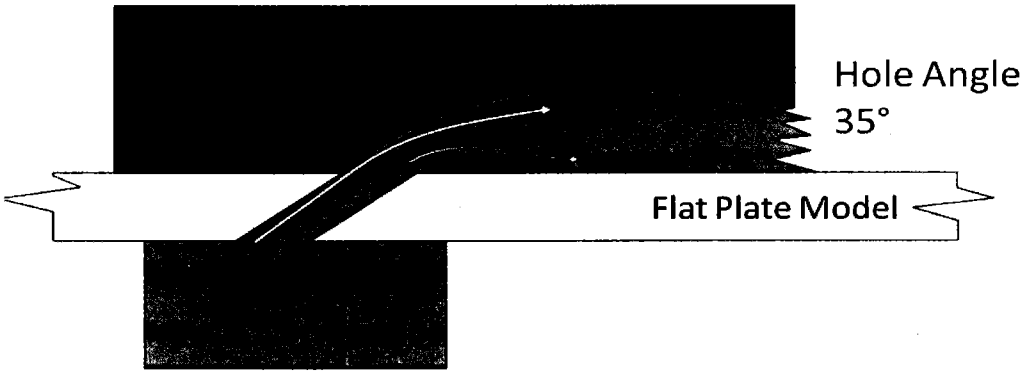

Figure 6 Schematic of Film Cooling Working Concept

1.2 Film Cooling

"Film cooling is the introduction of secondary fluid (coolant) at one or more discrete locations along a surface exposed to a high temperature environment to protect that surface not only in the immediate region of injection but also in the downstream region," [2]. The secondary air which is cool air were extracted from the compressor and injected near the blade surface (through holes or slots) to provide a layer of cool fluid between the hot gases and the blade surface thus reducing the heat transfer to the surface. Figure 6 illustrates the working principle of film cooling on flat plate model.

In general, the thermal protection provided by the film cooling is high close to the cooling hole and decreases progressively in downstream direction due to the mixing of cooling film and hot main flow. In comparison between the thermal protection provided by discrete cooling hole and a slot, the later is more efficient because the less intensive mixing process of the closed film ejected from a slot. However, high thermal stresses encountered on gas turbine blades and vanes do not allow the use of long slots. The modern film cooled turbine blades, therefore, are provided with rows of holes or rows of small slots. The investigation involving film cooling often prefers the flat surface model for its simplicity with the results obtained can be applied to real engine designs with slight corrections.

The effects of geometrical parameters like hole geometry, shape, size and spacing of the holes together with the flow parameters like coolant to mainstream mass flux ratio, temperature ratio, mainstream Reynolds number, velocity, and freestream turbulent intensity have been studied on flat surfaces. Latest reviews on the film cooling technology developments have been made by Bunker [3] covering most of the available film cooling technologies which are graded base on various factors; adiabatic effectiveness, manufacturability, cost, flow sensitivity etc.

In the real gas turbine, film cooling hole employed by the turbine components is either cylindrical or diffusion fan-shaped with 30° or 35° inclination relative to the protected surface along the streamwise direction. Full coverage thermal protection can prevail, if coolant flow attaches onto the protected surface and never penetrates and dissipates in the hot mainstream. However, such an ideal film cooling condition is always compromised because of the interaction between mainstream flow and the secondary air flow. Report of the early studies prevail a complex vortical structure in the wake of a transverse jet. This complex flow

pattern reflexes mainstream and secondary jet interaction and significantly affects film cooling performance. Generally, the inclined cylindrical cooling hole will generates counter rotating vortices which will persist until the hole exit. The initial generation of the counter rotating vortices will be help to continue its formation by the crossflow phenomena between the secondary air jets and the mainstream air. The counter rotating vortex pair, also known as kidney vortices tends to lift coolant flow off the protected surface and to entrain hot gases underneath as illustrated in Figure 7. As a result, coolant flow penetrates and dissipates quickly into the main flow stream, and degraded protection is inevitable. The degradation of the protection becomes worst at higher blowing ratio cases.

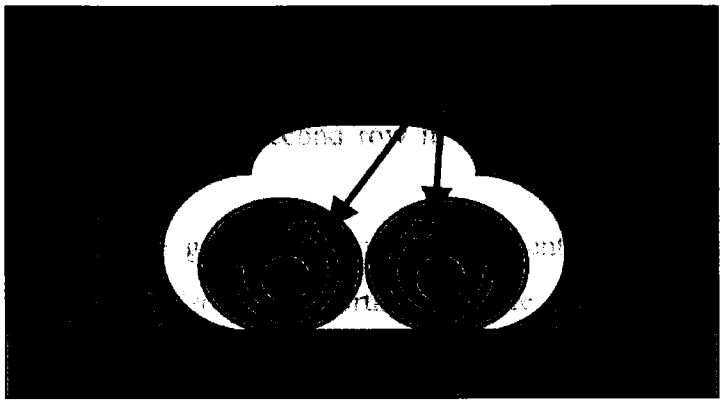

Figure 7 Idealized Shape of Cooling Jet with Symmetric Counter Rotating Vortices

1.3 Literature Review

Enormous numbers of experimental investigations dealing with both the aerodynamics and the thermal aspect of film cooling have been made available ever since and only a brief review will be provided in this paper. General review on flat plate surface film cooling studies prior to 1971 has been given by Goldstein [2]. Presented in the paper were the effects of various hole geometries and flow parameters that dictate the film cooling performance summarized from the prior available literatures [4–6]. Among the highlight of the paper are the superiority of inclined and shaped film cooling holes compared to perpendicular holes which contributes to momentum reduction at the hole exit due to wider exit area in inclined and shaped cooling hole which allows more coolant to remain attached to

the surface, leading to better the film cooling effectiveness with the shaped cooling hole also help to laterally diffuse the coolant to provide better lateral film cooling coverage. The same observation has been made by other researchers with further reduction on the hole angle expected to produce better film cooling performance. Although the advantages of the shaped holes is acknowledged, significant number of studies still focuses on cylindrical holes particularly on the hole geometry properties including compound angle [7–10] and hole length to diameter ratio [11, 12]. Jubran and Brown [13] and Ligrani et al. [8, 9] presented film cooling effectiveness of a multiple row cooling holes at different arrangement patterns. It was concluded that the two row cooling holes can significantly increase the laterally average cooling effectiveness either arranged in-line or staggered with the latter producing superior results. In the in-line arrangement, superposition effects result-in better film cooling effectiveness downstream of the second row holes and beyond. Meanwhile, wider film cooling coverage downstream of the second row in staggered hole arrangement led to the same consequences.

In addition to the hole geometries and arrangements, the amount of injected air through the cooling hole is also an important variable that decides the film cooling performance which is determine by blowing ratio. Considerable amount of investigations have been done to clarify the effects of blowing ratio to film cooling performance. To name one of the latest relevant studies is Rabekah et al. [14]. The paper presented the effect of various blowing ratio to the film cooling performance with the wall temperature data obtained by using temperature and pressure sensitive paints. The study shows the film cooling effectiveness is significantly influenced by the blowing ratio which generally agreed with the previous available findings [4, 5]. Base on the available observations and interpretations, film cooling performance of a given hole geometry, arrangement and flow condition are closely related to the flow structure of a given case, therefore investigation on the flow structure in the film cooling system is imperative.

The aerodynamics investigations of film cooling had started as early as 1980's with most of measurements were made by using the hot wire probe. It is found that phenomena such kidney vortices and flow separation plays a key role in film cooling performance. The kidney vortices as the prominent flow structure downstream of film cooling hole have been identified empirically by previous research [17–19], which concluded that the pair vortices entrain the mainstream fluid and transport it towards the blade surface. Recently, laser base

measurement instruments namely Particle Image Velocimetry (PIV) and Laser Doppler Velocimetry (LDV) have been utilized to capture flowfield as presented in the work of Thole et al. [20]. The paper presents the investigation on the flowfield of expanded exit cooling hole with comparison to the conventional cylindrical hole. Prediction on the film cooling performance have been made base on the interpretation of the measured flowfield. Film cooling performance of similar hole geometries have been published later by Gritsch et al. [21]. Good physical insight has been established between the aerodynamics [20] and thermal results [21]. Thole et al. [20] also highlighted the importance of understanding the inside hole flowfield as the hole exit flowfield is expected to play a major role on the formation of the downstream hole flowfield.

Wright et al. [22] on the other hand have presented the effect of mainstream turbulent level to the film cooling flow structure. The flow structure have been measured by using PIV on the plane normal to lateral direction to reflect the previous thermal study using the identical hole geometry. It was concluded that the main reason behind poorer film cooling performance at higher turbulent level is due to the enhancement of the mixing between the coolant and the mainstream air which lead to coolant temperature drop thus reducing its cooling capacity. Kampe et al. [23] presented a complete study of diffuser shape film cooling holes covering both the thermal and the aerodynamics aspects. The thermal measurements have been made by IR camera while both PIV and LDV have been used in the aerodynamics measurements. The paper also presented CFD results of the considered experimental condition. Physical interpretations on the film cooling performance have been made based on the aerodynamics results and a good agreement between the experimental and the CFD have also been achieved at the same time. The paper provides inclusive reviews of the diffuser shape film cooling holes.

1.4 Motivation

The present work, likewise in the efforts by Kampe et al. [23], aims at the clarification of detailed velocity field associated with cooling holes using 3D LDV and their characteristics in film effectiveness on the wall measured by IR camera. This present work especially deals with multiple cooling holes with in-line configurations. As mentioned in the previous section, there are several preceding studies on the in-line hole configuration, which

is usually for full coverage film cooling of combustor liners or turbine vanes. However, relatively few studies have been made on the in-line configuration in comparison with the staggered configuration because the former is believed to perform less than the latter. Nevertheless, it is still worthwhile to investigate in-line configuration of multiple cooling holes with some updated ideas in order to expand the design space of film cooling technologies. For this purpose, this study has consider multiple shallow cooling hole angle at 20 degree towards the streamwise direction performing in-line hole arrangements. The shallow hole angle of the cooling hole is predicted to provide better film protection in comparison to the common cooling hole having 35 degree hole angle.

1.5 Research Objectives

The objectives of the current study are:

a) To investigate the film cooling performance of multiple shallow cooling hole angle at 20 degree in comparison to the 35 degree cooling hole
b) To investigate the lateral pitch distance effect on film cooling performance of multiple shallow cooling hole at 20 degree
c) To investigate the flow structure of multiple shallow cooling hole angle at 20 degree in comparison to the 35 degree cooling hole
d) To investigate lateral pitch distance effect on the flow structure of multiple shallow cooling hole angle at 20 degree
e) To evaluate and manipulate the Computational Fluid Dynamics to provide further understanding on the aero-thermal interaction of shallow cooling hole angle at 20 degree

1.6 Research Frameworks

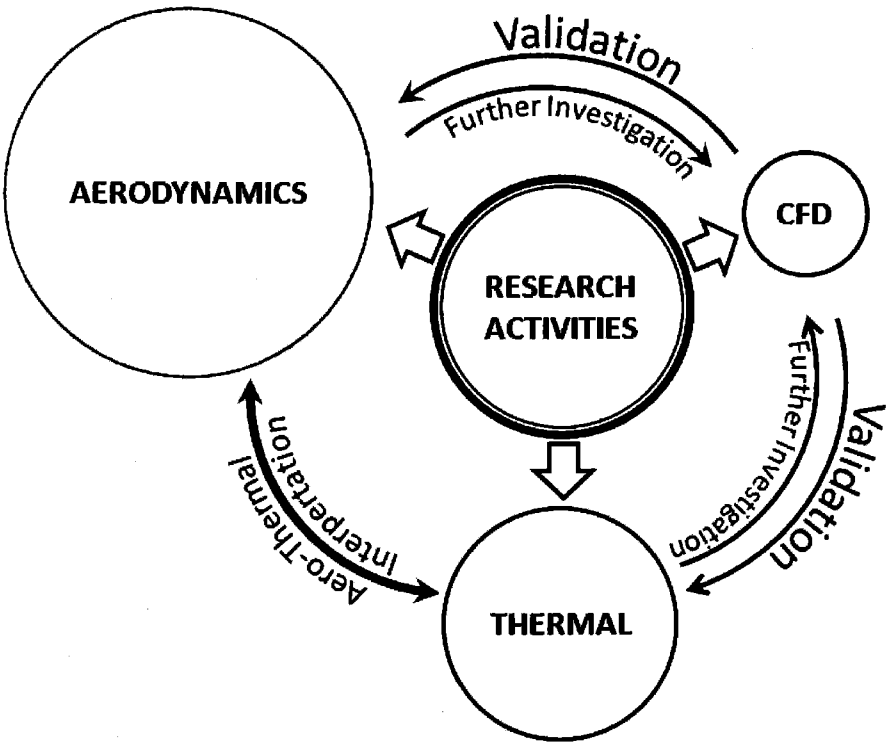

Figure 8 Overall View of the Research Framework

Figure 8 shows the overall view of the research framework of the present study. The present research activities consist of three main activities; a) Experimental Aerodynamic Investigations, b) Experimental Thermal Investigations; and c) Computational Fluid Dynamics Investigations involving both the aerodynamic and thermal aspects of the investigations. The experimental aerodynamic and the thermal investigations will be manipulate to understand the aero-thermal interaction of the given case. The aerodynamic results are expected to provide the physical phenomenon of a given thermal results. Both of the experimental results will be used to validate the capability of the computational fluid dynamics to predict the aero-thermal phenomena of the present study. In addition, the computational fluid dynamics will also be manipulated to provide details investigations on the aero-thermal phenomenon involved in the present study.

Chapter 2

Research Methodology

This chapter presents the research methodology implicated to the present study. The research method is divided into two; experimental and numerical investigation. The experiments discussed in this work involve two different experimental setups at Iwate University, Japan with each for the thermal and aerodynamic measurements. As both of these setups involved two different wind tunnels, two different experimental setups have been constructed. To make these thermal and aerodynamics results complementary to each other, the test models have been designed to have the same non-dimensional configuration which will be further discussed in this chapter. The chapter also provides details on the experimental work together on the description on the numerical work involve in the present study.

2.1 Test Model

Three test models have been considered in the present study namely Test Model A, Test Model B, and Test Model G. For the purpose of simplification, the test models will be referred to as TMA, TMB, and TMG respectively from now on in this writing. TMA, TMB and TMG consist of twenty cylindrical cooling holes arranged in five times four matrix performing an in-line hole configuration. Figure 9 associated with Table 1 described the geometry of the test models.

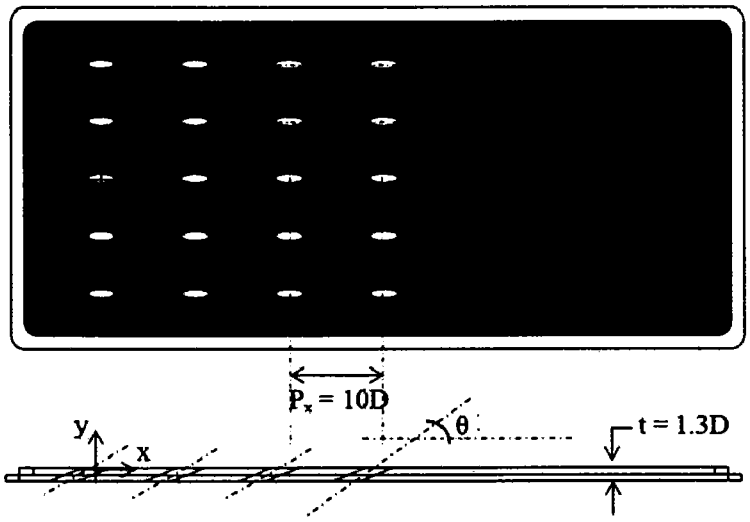

Figure 9 Details of the Test Model

Table 1 Details of the Test Model Geometries

	θ[°]	P_x	P_z	t	l
TMA	20	10D	6D	1.3D	3.81D
TMB	35	10D	6D	1.3D	2.27D
TMG	20	10D	3D	1.3D	3.81D

Based on the current available literature, TMB was designed to be a baseline test model with 35° hole angle in the streamwise direction. TMA and TMG are both having shallow hole angle imbedded at 20° hole angle in the streamwise direction. The thickness of the test models has been fixed at, t = 1.3D which consequently will provide a hole length, l= 3.81D for TMA and TMG, and l = 2.27D for TMB. As been mentioned previously, since the experiments involved two different wind tunnels, the test models have been designed to have the same non-dimensional configuration base on the cooling hole diameter with the aerodynamics and thermal investigations are having the diameter of the cooling hole at, D = 10mm and 7mm respectively. The overall size of the test model was determined in consideration of the possible development of film cooling effectiveness region further downstream of the last row of the cooling holes. The test models were made from medium impact acrylic plate with thermal conductivity, k = 0.19 W.m^{-1}K^{-1}. The inner surface of the test models were coated with black paint to emulate a black body in the thermal measurements and to reduce the surrounding noise during the aerodynamic measurements

caused by laser reflection. All test models have been considered in thermal investigations and only TMA, TMB and TMG were considered for aerodynamics investigations. Figure 10 shows the entire test model involved in the present study.

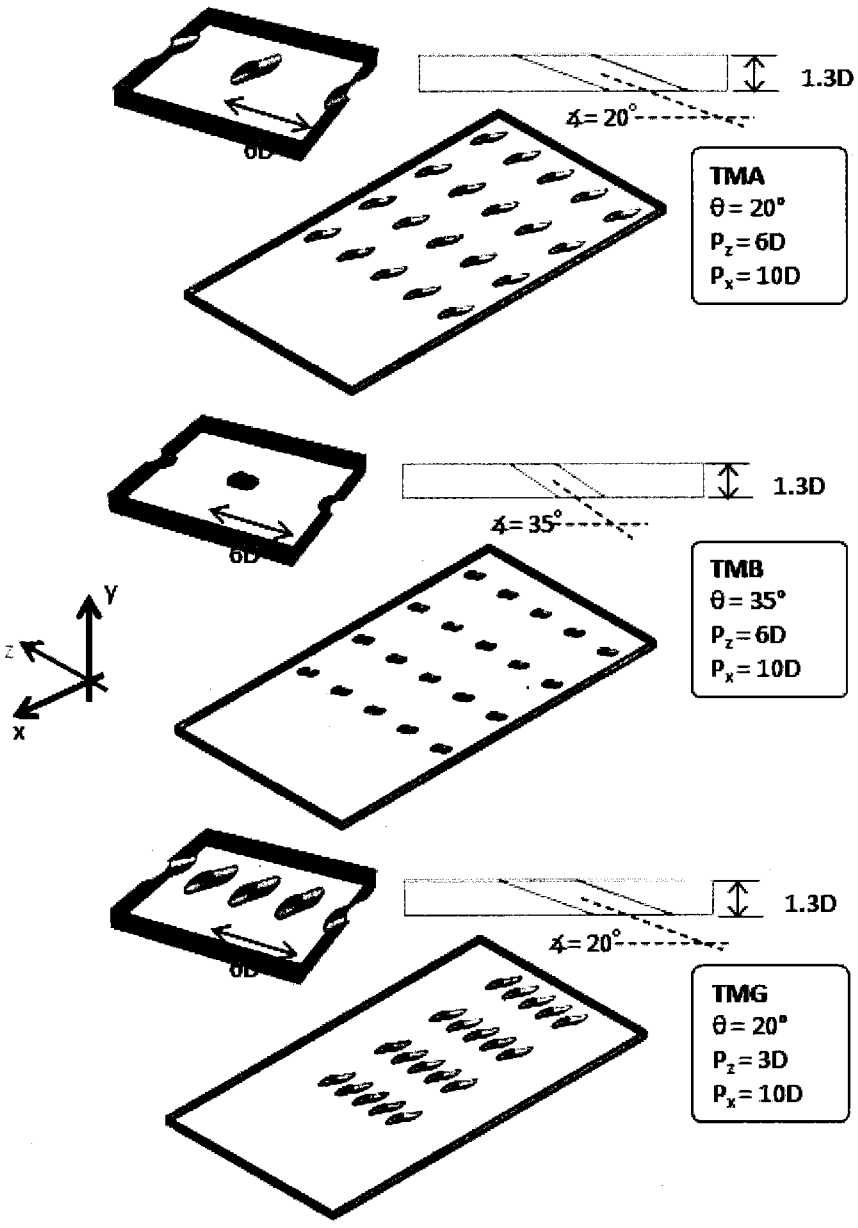

Figure 10 Overall View of the Test Models

2.2 Experimental Condition

All the experiments have been conducted at single targeted Reynolds number base on the hole diameter, $Re_D = 6200$. The definition of the Reynolds is given by Eq. (2)

$$Re_D = \frac{\rho_\infty \cdot U_\infty \cdot D}{\mu} \tag{2}$$

where;

ρ_∞, mainstream air density, [$kg.m^{-3}$];

U_∞, mainstream air velocity [$m.s^{-1}$];

D, cooling hole diameter [m]; and,

μ , mainstream air viscosity [$kg.m^{-1}.s^{-1}$]

The Reynolds number involved in the real gas turbine is far exceeding the considered value in the present study. Due to the limitations of the experimental setup, only such Reynolds number can be considered in the present study. Another fundamental variable in the film cooling study that have been considered in the is blowing ratio, *BR* which is define by Eq. (3),

$$BR = \frac{U_c \cdot \rho_c}{U_\infty \cdot \rho_\infty} \tag{3}$$

where;

U_c, secondary air hole exit velocity, [$m.s^{-1}$];

ρ_c , secondary air density, [$kg.m^{-3}$];

U_∞, ; mainstream velocity, [$m.s^{-1}$]; and,

ρ_c;. mainstream air density, [$kg.m^{-3}$].

At the initial stage of the study, three blowing ratios have been considered at BR = 0.5, 1.0 and, 2.0. However, higher blowing ratios have been considered in the later stage. The consideration of higher blowing ratio was made due to the promising thermal results that have obtain in the case of shallow hole angle configuration. Details on the high blowing ratio cases have been presented in the last chapter of this writing.

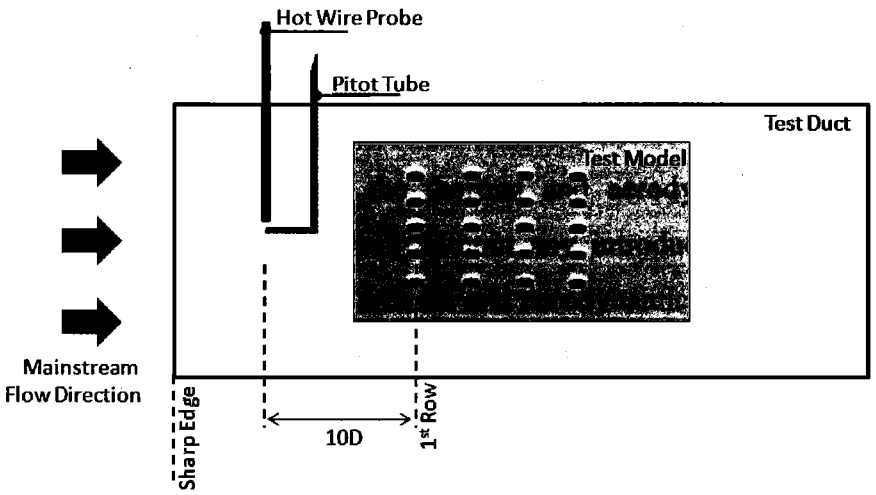

Figure 11 Mainstream Turbulent Intensity Measurement

Table 2 Experimental Matrix of the Present Study

		Aero	Thermal
TMA	BR05		O
	BR10	O	O
	BR20	O	O
TMB	BR05		O
	BR10	O	O
	BR20		O
TMG	BR05		O
	BR10	O	O
	BR20	O	O

To provide more information involving the flow characteristics involve in the present study, the turbulence intensity of the mainstream flow have been measured. The mainstream turbulence level for the thermal investigations is measured to be at, Tu = 0.13%, while for the aerodynamics investigations the turbulent intensity measured to be at, Tu = 0.15%. The mainstream turbulent level for both the thermal and aerodynamics setup are naturally established in the mainstream flow path without any introduction of turbulent promoter. Although the turbulence levels of the thermal and aerodynamics investigation do not match each other, nevertheless at the same order of magnitude, the freestream turbulence effect on the film cooling effectiveness and secondary flowfield of the present study could be assume at minimum. The turbulence intensity level was measured by a hot wire probe at location of x/D = 10 upstream of the first row cooling hole. Figure 11 shows the schematics diagram of the mainstream turbulent measurement, meanwhile Table 2 shows the experimental matrix involved in the present study.

2.3 Aerodynamics Investigation

2.3.1 Overall Setup

The aerodynamics investigations involved in the present study have been carried out in a large-scale close-loop wind tunnel. Figure 12 shows the overall view of the experimental setup. The mainstream air was supplied into the test section by a centrifugal blower via settling duct, flow contraction nozzle, straighteners, and transition duct. The test duct size at 620mm x 260mm inlet dimension with 1550mm length. The secondary air was supplied through a separate blower equipped with a laminar flow meter. After passing the laminar flow meter, the secondary air will entered a secondary air chamber before being introduced into the mainstream flow through the cooling hole. The view of the test duct together with the positioning of the laser probe involved in the measurement is shown in Figure 13. The orientation of the test duct made the test model surface to be perpendicular to the ground level. Such orientation was necessary to enable the Laser Doppler Velocimeter (LDV) probe to access the desired measurement locations.

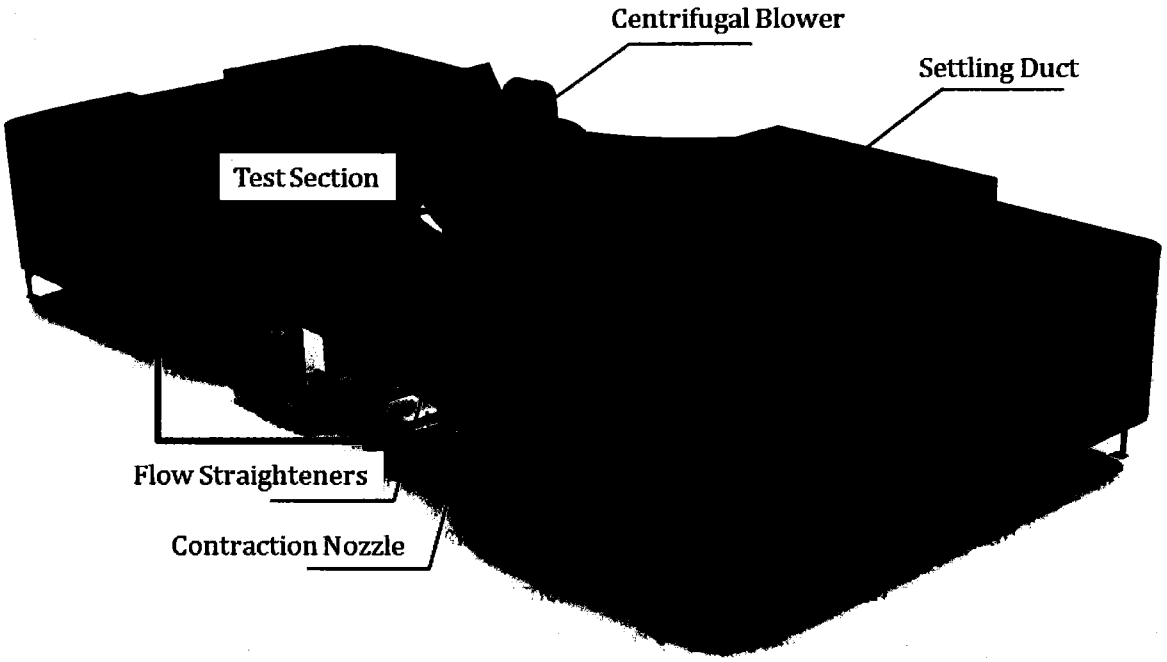

Figure 12 Overall View of the Aerodynamics Experimental Setup

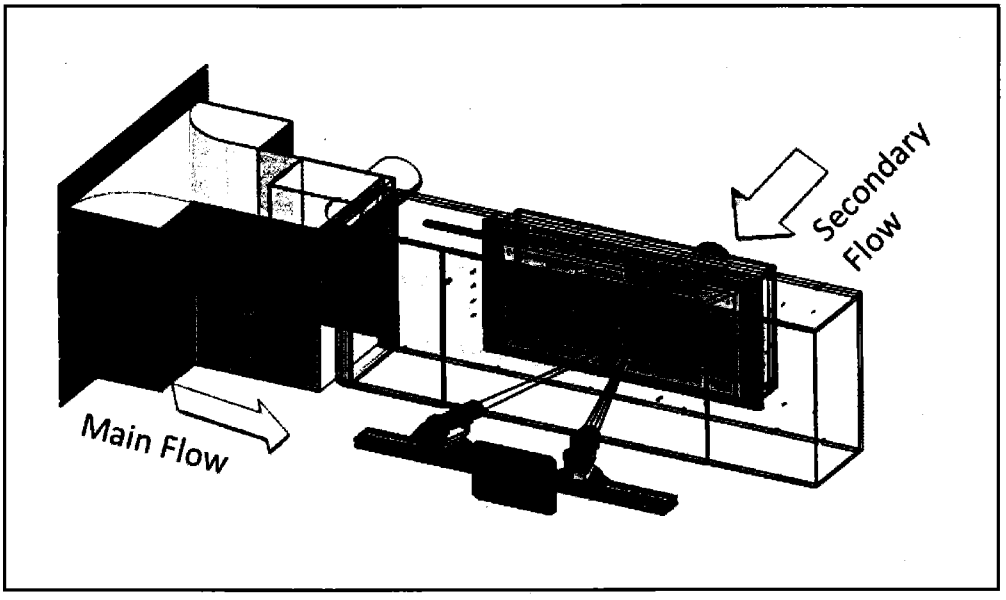

Figure 13 View of the Test Section for Aerodynamics Investigation

2.3.2 Velocity Field Measurement

A three-component Laser Doppler Velocimetry (LDV) was used to capture the velocity fields of the present study. The LDV system engaged includes 85mm fiber optic probe, Dantec's BS F60 Processor and 3D Traversing System provided by Dantec. The laser probes traveled by the traverse system will go through a set of measurement points performing a plane grid which is shown in Figure 14. The measurement plane is covering the lateral distance at $3.6 < z/D < -3.6$ and $2.3 < y/D < 0.3$ in the vertical direction. The size of the measurement plane was decided base on the preliminary measurement with intention avoiding insignificant area to be involved in the actual measurement. The measurement grid size applied on the plane is set to be at 2mm times 2mm which been proved to be small enough to capture the flow details also during the preliminary measurement. Several measurement planes have been considered at x/D = 3, 7, 13, 17, 23, 27, 33 and 37 as been shown in Figure 15. During the measurements, both the mainstream and the secondary air were seeded with particles produced by the SAFEX Fog Generator (Figure 16) at average droplet size diameter of 1.545μm. The seeding particles were supplied through a fog tank to ensure continuous supply of the fog during the experiments. The uniformity of the seeding particle distribution was ensured through the data rate distribution on the measurement plane during the preliminary measurement.

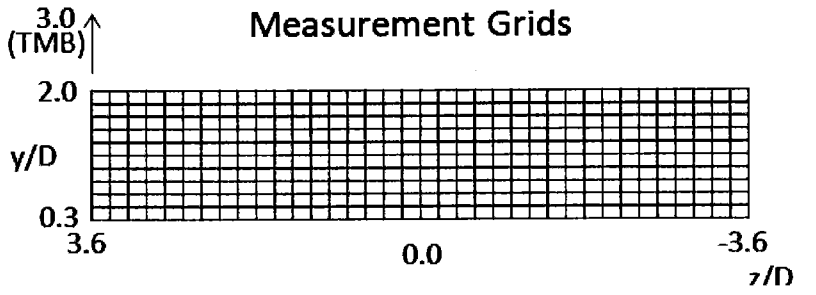

Figure 14 Measurement Grid

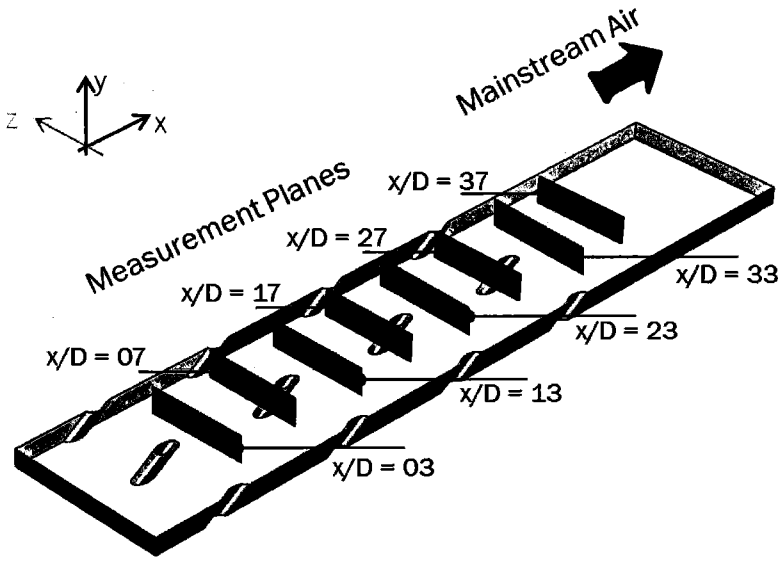

Figure 15 Aerodynamics Measurement Planes

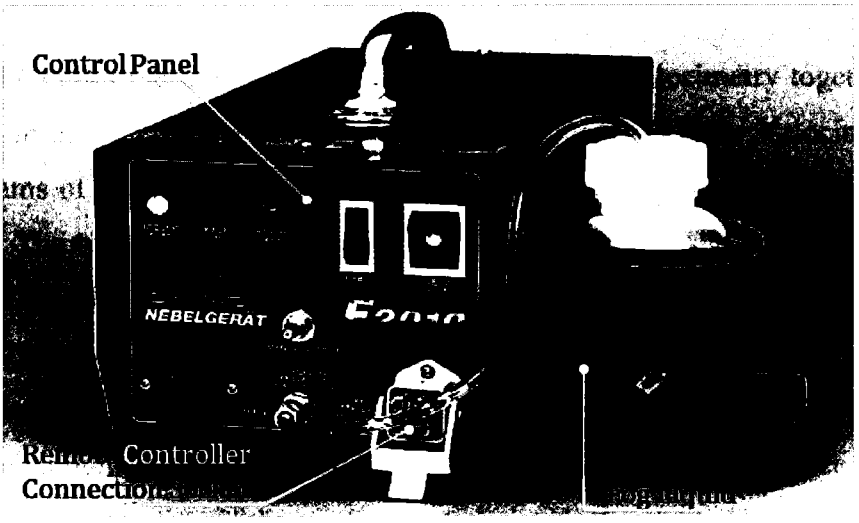

Figure 16 Fog Generator

2.3.3 Laser Doppler Velocimetry

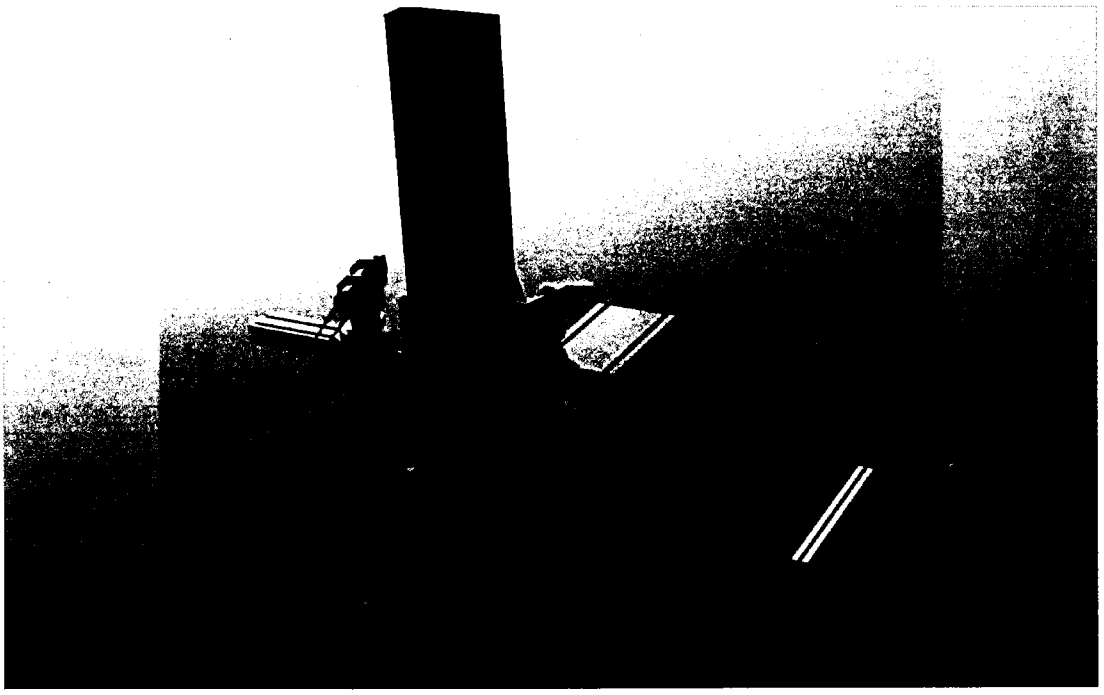

Figure 17 3D Laser Doppler Velocimetry and Traverse System

Figure 17 shows the three dimensional Laser Doppler Velocimetry together with the traverse system in used of the present study. In principle, Laser Doppler Velocimetry (LDV) crosses two beams of collimated, monochromatic, and coherent laser light in the flow of the measured fluid. The two beams are obtained by splitting a single beam and at the same time maintaining the coherence between the two. The lasers have the wavelengths in the visible spectrum (390-750 nm); allowing the beam path to be observed. A transmitting optics focuses the beams to intersect at a focal point, where the interference between the laser beams generate a set of straight fringes also known as laser volume in the case of three dimensional measurement. The intervention of the seeding particle inside the created laser volume enables the laser to obtain a feedback which is interpreted as velocity component, u, v, and w in *x*-direction, *y*-direction and *z*-direction respectively. Figure 18 illustrates the overall working concepts of LDV. The velocity components were estimated based on the statistical data of the seeding particle that get intact with the laser volume. The numbers of counts involved during the measurement was set to be at minimum of 750 counts, while almost all the considered measurement points recorded the counts value above 1000 counts.

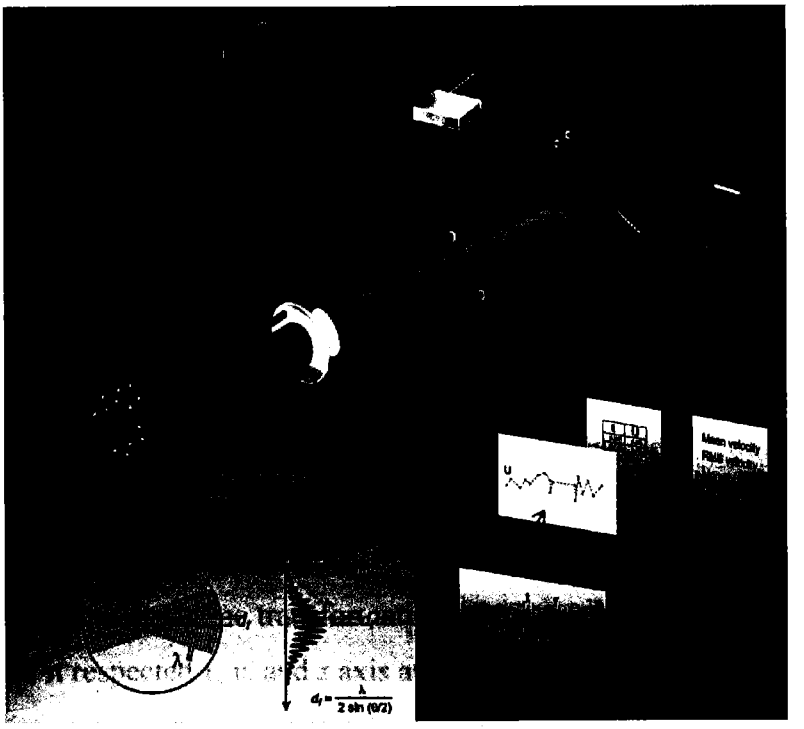

Figure 18 Working Concepts of Laser Doppler Velocimetry

Eq. (4) and Eq. (5) defines the formula for time average and root means square (RMS) value of velocity components, respectively.

$$\overline{U}_{x,y,z} = \frac{1}{N}\sum_{i=1}^{N} U_i \tag{4}$$

$$RMS_{u,v,w} = \sqrt{\frac{1}{N-1}\sum_{i=1}^{N}\left(U_i - \overline{U}_{x,y,z}\right)^2} \tag{5}$$

where;

x, y, z, coordinate axis, [-];

N, number of count, [-];

U_i, instantaneous velocity, [m.s^{-1}]

In addition to the above mentioned variables, by using the coincident data measurement method, the value of Reynolds stress tensor can also be generated from the measured LDV data which is determine by Eq. (6) and Eq. (7).

$$\overline{u'v'} = \frac{1}{N}\sum_{i=1}^{N}(u_i - \bar{u})(v_i - \bar{v}) \tag{6}$$

$$\overline{u'w'} = \frac{1}{N}\sum_{i=1}^{N}(u_i - \bar{u})(w_i - \bar{w}) \tag{7}$$

2.3.4 Transformation Matrix

To enable the interference between the laser beams, the probes were set to be inclined at 25° towards each other as shown in Figure 17. The alignment requires the measured velocities (u_1, u_2 and u_3) to go through a transformation process to represent the velocity components of the actual experimental axis. The transformation is done through the BSA Flow Software with the user define transformation matrix as shown in Eq. (8) where u, v and w is the velocity of it respected x, y, and z axis and C_{11}, C_{12}, … and C_{33} are the transformation coefficients.

$$\begin{bmatrix} u \\ v \\ w \end{bmatrix} = \begin{bmatrix} C_{11} & C_{12} & C_{13} \\ C_{21} & C_{22} & C_{23} \\ C_{31} & C_{32} & C_{33} \end{bmatrix} \begin{bmatrix} u_1 \\ u_2 \\ u_3 \end{bmatrix} \tag{8}$$

Base on the probe inclination on the x-axis, the coefficient matrix can be written as Eq. (9) where the $\alpha_1$and $\alpha_2$are the inclination angle of the probe on the x-axis.

$$C = \begin{bmatrix} 1 & 0 & 0 \\ 0 & \dfrac{\sin\alpha_2}{\cos(\alpha_1+\alpha_2)} & \dfrac{\sin\alpha_1}{\sin(\alpha_1+\alpha_2)} \\ 0 & \dfrac{\cos\alpha_2}{\sin(\alpha_1+\alpha_2)} & \dfrac{-\cos\alpha_1}{\sin(\alpha_1+\alpha_2)} \end{bmatrix} \tag{9}$$

given$\alpha_1 = \alpha_2 = \alpha$, the transformation coefficient matrix can be simplified to Eq. (10)

$$C = \begin{bmatrix} 1 & 0 & 0 \\ 0 & \dfrac{1}{2\cos\alpha} & \dfrac{1}{2\cos\alpha} \\ 0 & \dfrac{1}{2\sin\alpha} & \dfrac{-1}{2\sin\alpha} \end{bmatrix} \tag{10}$$

2.4 Thermal Investigation

2.4.1 Overall Setup

Figure 19 shows the experimental setup for thermal investigation involved in the present study. The facility consists of a wind tunnel used to supply the mainstream air representing the hot gas in the real gas turbine operation. A separate blower is used to supply the secondary air. The test duct cross section was designed to have 450mm width and 280mm height with a sharp upstream edge to recreate the boundary layer inside the test section. The overall size of the test model for the thermal investigation was set to be at 250mm x 545mm with the hole diameter of 7mm. The size of the test model was determined in consideration of the possible development of film cooling effectiveness region further downstream of the last row of the cooling holes. Insulation layer have been fix at the back of the test model to avoid heat conduction from secondary air chamber to the test model. Figure 20 shows a close up view of the test section for thermal investigation.

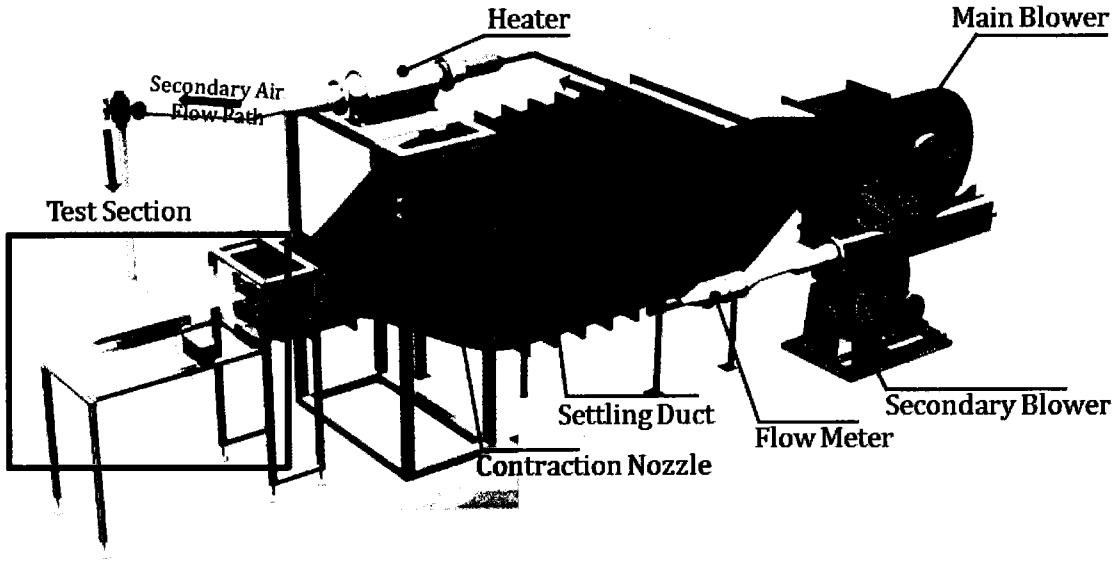

Figure 19 Overall View of the Thermal Experimental Setup

References

[1] Han, J.C., Dutta, S., and Ekkad, S, 2000, "Gas Turbine Heat Transfer and Cooling Technology," Taylor and Francis, New York, pp. 129-436.

[2] Goldstein, R.J., Eckert, E.R.G., Tsou, F.K., and Haji-Sheikh, A., 1971, "Film Cooling," *Advances in Heat Transfer*, Vol. 7, pp. 32–379.

[3] Bunker, R.S., 2009 "Film Cooling: Breaking the Limits of Diffusion Shaped Holes," *Proceeding of International Symposium on Heat Transfer in Gas Turbine System*, Antalya, Turkey.

[4] Goldstein, R.J., Eckert, E.R.G., and Ramsey, J.W., 1968, "Film Cooling with Injection Through Holes: Adiabatic Wall Temperature Downstream of a Circular Hole," *J. Eng. Power*, Vol. 90, pp. 384-395.

[5] Goldstein, R.J., Eckert, E.G., Eriksen, V.L., and Ramsey, J.W., 1970, "Film-cooling Following Injection through Inclined Circular Tubes," *Israel J. Technology*, Vol. 8, pp.145-154.

[6] Goldstein R.J., Eckert, E.R.G., and Burggraf, F., 1974, "Effect of Hole Geometry and Density on Three Dimensional Film Cooling," *Int. J. Heat Mass Transfers*, Vol. 17, pp. 595-607.

[7] Gustafsson, K.M.B, and Johansson, 2001, "An Experimental Study of Temperaure Distribution on Effusion-Cooled Blade," *ASME J. Engineering for Gas Turbines and Power*, Vol. 123, pp.308-316.

[8] Ligrani, P.M., Wingle, J.M., Ceriello, S., and Jakson, S.W., 1994, "Film Cooling from Holes with Compound Angle Orientations Part 1: Results Downstream of Two Staggered Rows of Holes with 3d Spanwise Spacing," *ASME J. Heat Transfer*, Vol. 116, pp. 341–352.

[9] Ligrani, P.M., Wingle, M., and Jakson, S.W., 1994, "Film Cooling from Holes with Compound Angle Orientations Part 1: Results Downstream of Two Staggered Rows of Holes with 6d Spanwise Spacing," *ASME J. Heat Transfer*, Vol. 116, pp. 353–362.

[10] Goldstein, J.R., and Jin, P., 2000, "Film Cooling Downstream of a Row of Discrete Holes with Compound Angle," *ASME J. Turbomachinery*, Vol. 123, pp. 222-230.

[11] Lutum, E., and Johnson, B.V., 1998, "Influence of the Hole Length-to-Diameter on Film Cooling with Cylindrical Holes," *ASME J. Turbomachinery*, Vol. 121, pp. 209-216.

[12] Burd, S.W., Kaszeta, R.W., and Simon, T.W., 1998, "Measurement in Film Cooling Flows: Hole L/D and Turbulent Intensity Effects," *ASME J. Turbomachinery*, Vol. 120, pp.791-798.

[13] Jubran, B., and Brown, A., 1985, "Film-cooling From Two Rows of Holes Inclined in the Streamwise and Spanwise Directions," *ASME J. Engineering Gas Turbines Power*, Vol. 107, pp. 84–91.

[14] Rebekah A.R., Alfred, D., and Wright, L.M., 2009, "Measurement of Details Heat Transfer Coefficient and Film Cooling Effectiveness Distribution using PSP and TSP," *Proceeding of ASME Turbo Expo*, GT2009–59975

[15] Cho, H.H., Rhee, D.H., and Kim, B.G., 2001, "Enhancement of Film-cooling Performance Using a Shaped Film-cooling Hole with Compound Angle Injection," *JSME International Journal*, Series B, Vol. 44, No. 1, pp. 99–110.

[16] Sinha, A.K., Bogard, D.G., Crawford, M.E., 1991, "Film Cooling Effectiveness Downstream of a Single Row of Holes with Variable Density Ratio," *ASME J. Turbomachinery*, Vol. 113, pp. 442–449.

[17] Andreopoulus, J., and Rodi, W., 1984, "Experimental Investigation of Jets in a Crossflow," *J. Fluid Mechanics*, Vol. 138, pp. 93–127.

[18] Subramaniam, C.S., Ligrani, P.M., Green, J.G., Doner, W.D., and Kaisuwan, P., 1992, "Development and Structure of a Film-Cooling Jet in a Turbulent Boundary Layer with Heat Transfer," *Proceeding of the 3rd International Symposium on Transport Phenomena and Dynamics of Rotating Machinery*, pp. 53–68.

[19] Pietrzyk, J.R., Bogard, D.G, and Crawford, M.E., 1989, "Hydrodynamic Measurements of Jets in Crossflow for Gas Turbine Film Cooling Application," *ASME J. Turbomachinery*, Vol. 111, pp. 139-145.

[20] Thole, K., Gritsch, M., Schulz, A., and Wittig, S., 1996, "Flowfield Measurements for Film-Cooling Holes with Expanded Exits," *Proceeding of International* Gas *Turbine and Aeroengine Congress and Exhibition*, 96-GT-174.

[21] Gritsch, M., Schultz, A., and Witting, S., 1998, "Adiabatic Wall Effectiveness Measurements of Film-Cooling Holes with Expanded Exit," *ASME J. Turbomachinery*, Vol. 120, pp. 549-556.